A satellite altimeter model for ocean slick detection

J. Tournadre,[1] B. Chapron,[1] N. Reul,[1] and D. C. Vandemark[2]

Received 20 June 2005; revised 28 November 2005; accepted 23 December 2005; published 11 April 2006.

[1] About 5% of Ku-band altimeter ocean data are degraded by the occurrence of high radar return cross sections (σ_0), usually called σ_0 blooms. During blooms, which occur during no or low wind conditions, the mean altimeter waveform can significantly depart from the expected shape. In about 60% of the cases the waveforms are distorted to such an extent that either the range tracker loses lock or the off-nadir angle estimate becomes unrealistic. The analysis of high data rate altimeter waveforms during bloom events reveals the presence of V-shaped patterns similar to the ones observed during rain events. These patterns trace small-scale (i.e., smaller than the altimeter footprint) changes in surface backscatter. Such variations of surface roughness are commonly observed in SAR images under low wind conditions. On the basis of the experience gained through the analysis of high-resolution altimeter waveforms in the presence of rain cell, a model is developed to analyze the altimeter response to phenomena whose length scale is smaller than the altimeter footprint. The model is applied to simple patterns (linear slicks and circular patches) as well as to realistic surface σ_0 estimated by SAR. It is also used to analyze bloom events in terms of surface slicks. The model results shows that the small-scale σ_0 variations explain the behavior of altimeter waveforms in bloom events. The results also show that a good proportion of data during bloom events are still valid for estimating geophysical parameters as the Brown model remains valid. Use of high-resolution altimeter waveforms may also offer an interesting mean to study marine slick occurrence rates and type.

Citation: Tournadre, J., B. Chapron, N. Reul, and D. C. Vandemark (2006), A satellite altimeter model for ocean slick detection, *J. Geophys. Res.*, *111*, C04004, doi:10.1029/2005JC003109.

1. Introduction

[2] Satellite altimetry has become a standard tool for geophysicists, including oceanographers, geodesists, and solid earth physicists. Over the oceans, satellite altimeters provide measurements of the sea surface height, the significant wave height and the backscatter of the sea surface from which wind speed can be inferred [*Brown*, 1977]. Precise determination of these values, especially the topography, is critical to the success of the satellite mission. As usually found, roughly 5% of all Ku band altimeters (TOPEX/Poseidon, Jason or Envisat) ocean data exhibit a phenomenon that has been called "σ_0 bloom" by various authors, for example, recently *Mitchum et al.* [2004] and *Tran et al.* [2002]. These blooms are regions characterized by unusually high values of the ocean surface radar backscatter cross section. As anticipated by *Brown* [1979], such events shall occur during low wind and sea state conditions. In regions where Ku-band σ_0 exceeds 14 dB, the altimeter mean return waveform shape can significantly depart from its expected shape and the off-nadir angle obtained from the shape of the return waveform can become unreliable. This can trigger an attitude estimation error and the average waveform during bloom events presents an excessive decay in the waveform plateau. *Brown* [1979] suggested that these cases might provide a unique opportunity estimate of the probability density function of the slopes of the low sea state surface waves. However, this breakdown in the waveform model is likely to be associated with strongly inhomogeneous surface conditions. Indeed, under extremely calm surface conditions, surface slick patches are commonly observed. For example, synthetic aperture radar (SAR) imagery exhibits a very wide range of spatial scales for which the ocean surface provides little or no surface reflection back to the radar, indicating that centimeter scale wavelets are absent on the surface [*Clemente-Colón and Yan*, 2000]. Consequently, a fraction of the probed surface area will provide an extremely high altimeter cross section. The altimeter waveform will thus be modified. The distortion of the waveform can be such that the altimeter range tracker can lose lock leading to data losses. More interestingly, blooms may provide the opportunity to study the frequency, occurrence and extent of sea surface calms, possibly associated with slick formation.

[3] To advance in σ_0 bloom analysis, we thus proposed to revisit the analysis of altimeter waveforms. Standard analysis is based on the *Brown* [1977] rough surface model which states that the return power is the convolution of three terms, i.e., the point target response (PTR), which represents the original pulse, the flat surface response, which includes

[1] Laboratoire d'Océanographie Spatiale, Institut Français de Recherche pour l'Exploitation de la Mer, Plouzané, France.
[2] NASA Goddard Space Flight Center, Wallops Island, Virginia, USA.

0148-0227/06/2005JC003109$09.00

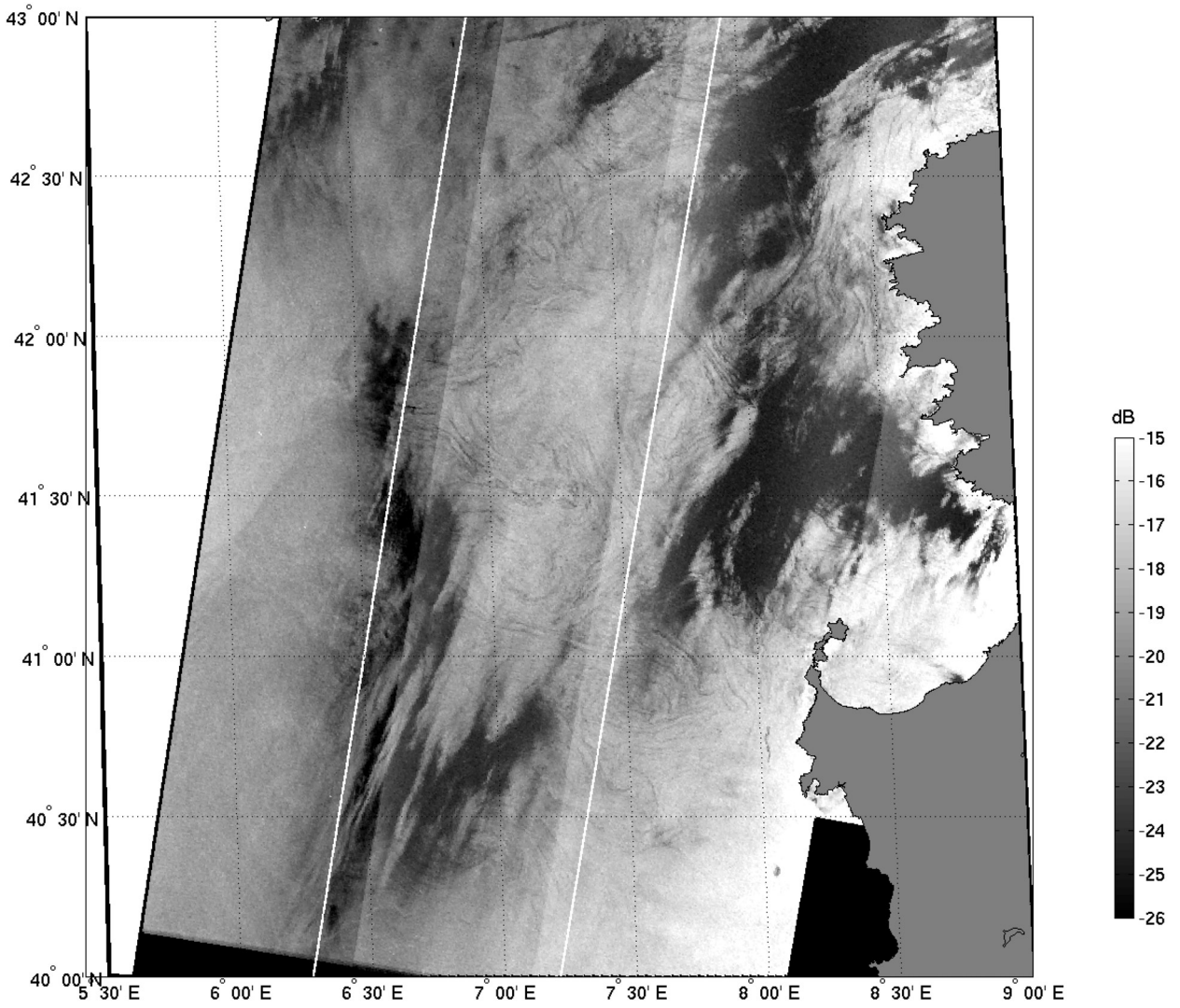

Figure 1. Radarsat Image taken on 24 April 2004 off the coast of Corsica under low wind speed conditions (less than 1.5 m/s) showing zone of little backscatter (dark patches) and slick-like features.

the altimeter antenna pattern and the probability density function of the specular heights. One basic assumption of this model is the homogeneity of the sea surface roughness (i.e., of surface σ_0) within the altimeter footprint. This assumption is, in general, true under normal winds conditions; that is, wind variations within the footprint gives small σ_0 variations. However, as stated above, under very low wind conditions, the nadir σ_0 can be highly dynamic owing to small variation in surface wind/roughness conditions. An example of SAR imagery under low wind conditions clearly shows that strong variations of surface σ_0 at length scales smaller than the altimeter's 4- to 5-km-radius footprint can occur (see Figure 1). These strong σ_0 variations will strongly modify the shape of the altimeter waveforms in a manner similar to that already demonstrated in case of rain [*Tournadre*, 1998]. Indeed, in the presence of rain cells, it is not the surface σ_0 that is modified but the atmospheric attenuation. However, the resulting effect is similar. We thus propose to adapt these rain-based developments to the σ_0 bloom analysis. In particular, we emphasize that only high data rate altimeter waveforms are adapted to analyze the altimeter response to phenomena whose characteristic length scales are smaller than the altimeter footprint.

[4] In their study of σ_0 bloom events, *Mitchum et al.* [2004] only used 1-second average waveforms which might explain why they failed to reproduce such waveform behavior. An example σ_0 bloom presented in Figure 2 shows the complexity of the phenomenon. This σ_0 bloom event was detected in the Jason archive (cycle 10 pass 17) off the coast of Sumatra. Between 2°S and the Equator, Ku band σ_0 presents large variation and greatly exceeds 20 dB in most of the zone. The high rate (20Hz) waveforms show a large proportion is distorted. The α-β tracker experiences problems in detecting the waveform leading edge (which should be normally centered at the telemetry sample 32.5). This is particularly obvious near 1.65°S or 1.2°S. The distortion of the waveform and the tracker loss result in data flagging for bad quality in the satellite's Geophysical Data Record. The flagged samples are indicated by red

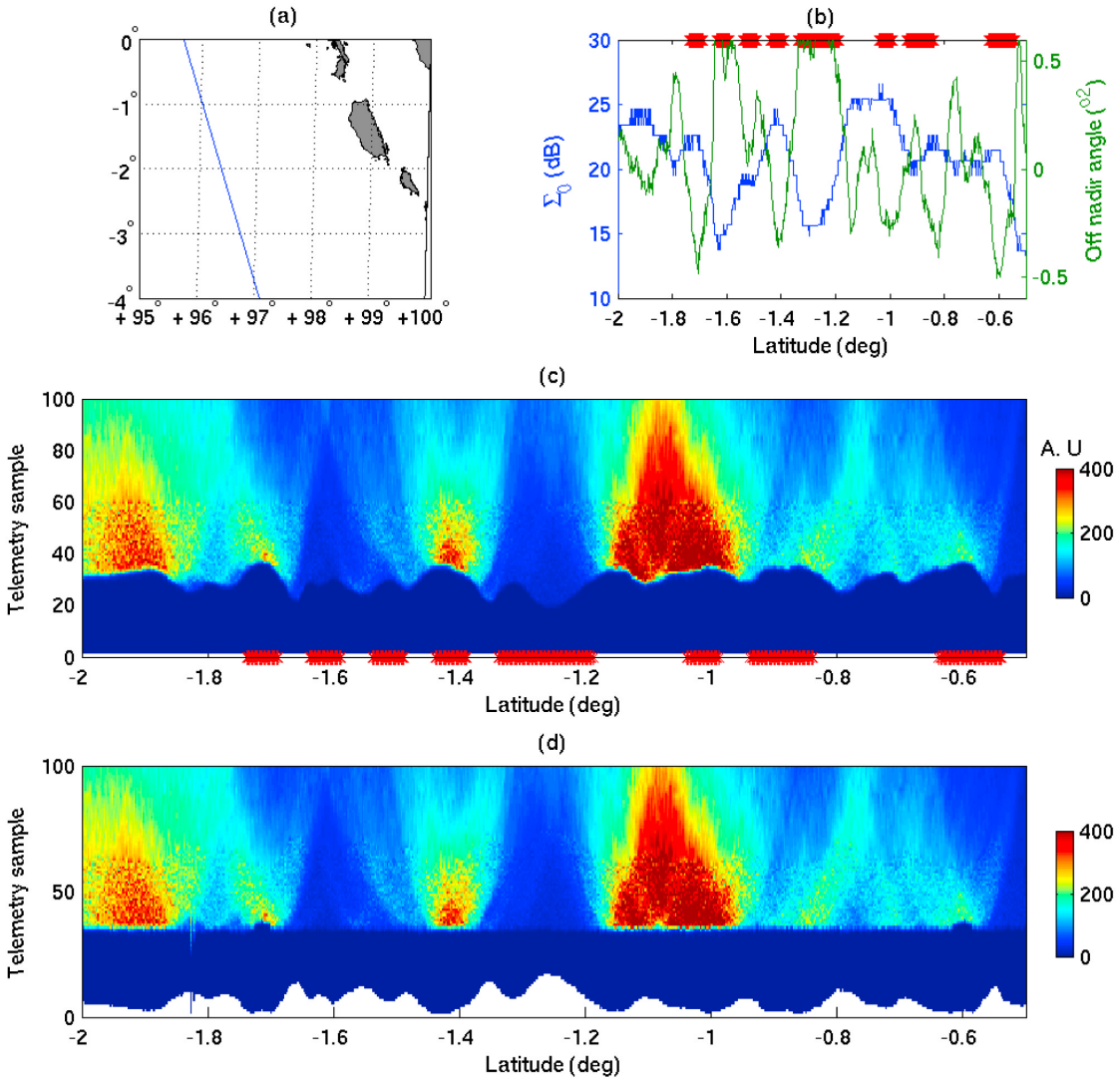

Figure 2. Example of σ_0 bloom event off the coast of Sumatra, Jason cycle 107 orbit 14. (a) Jason ground track, (b) Ku band σ_0 and off-nadir angle, (c) 20-Hz altimeter waveforms (raw), and (d) retracked 20-Hz altimeter waveforms. The waveform colorscale is in Arbitrary units. The red asterisks mark the samples that are flagged for errors in the Jason Geophysical Data Records.

asterisks. More interestingly, the waveform field features V-shaped (parabola like) patterns of enhanced backscatter such as the one that can be seen near 1.4°S. V-shaped patterns of attenuated backscatter were also detected in case of rain events. These patterns trace in surface σ_0.

[5] When the tracker lock is lost, the waveforms are artificially shifted to smaller time. The leading edge of the waveforms is in general still present in the data, but misplaced. It is thus possible to retrack the waveforms using a procedure based on the detection of the leading edge such as the one proposed by *Tournadre* [1998]. For retracked waveforms, also presented in Figure 2 the V-shaped patterns appear more clearly, for example, the three seen between 1.8 and 1.7°S.

[6] The off-nadir angle, i.e., the depointing angle of the altimeter radar, estimated from the slope of the retracked waveform plateau (see method in section 3) also exhibits large oscillations which indicates strong departure from the theoretical model. The mean normalized waveforms for σ_0 greater than 20 dB presented in Figure 3 experience a more rapid plateau decay when compared to the normal waveform (σ_0 < 16 dB) as in the work of *Mitchum et al.* [2004]. This average behavior conceals part of the complexity that is observed in the waveforms of Figure 2. The waveforms can also be sorted according to the satellite waveform retrieved off-nadir angle which is a better indicator of the waveform shape than σ_0. For small off-nadir angle (<0.1°²), the mean normalized waveform is similar to the theoretical one. For large negative values (<-0.2°²) and σ_0 > 20 dB, the mean waveform presents a very steep decay of the plateau and high peak near the maximum amplitude. For large positive values (>0.2°²) and σ_0 > 20 dB, the mean waveform presents an inverse behavior, increasing plateau and low peak. The apparent similarity of behavior between rain and bloom cases suggests there is a methodology available to describe the strong variability of the surface σ_0 to model

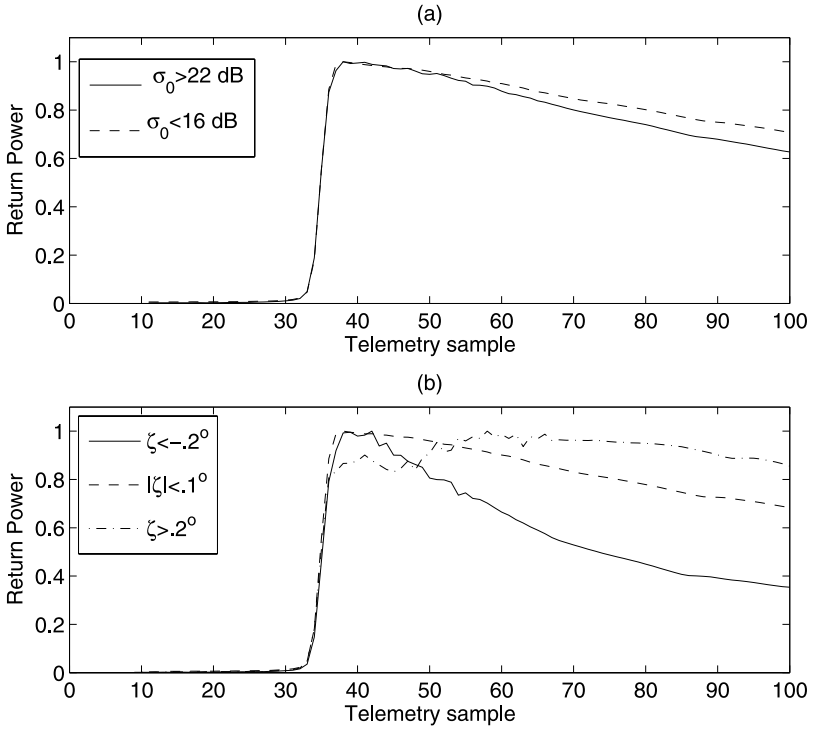

Figure 3. Mean normalized altimeter waveforms (a) sorted according to σ_0 and (b) sorted according to the off-nadir angle.

altimeter waveforms. This model is presented in section 2. The model is then applied to the simple case of a linear surface slick within the altimeter footprint. Section 3 compares the modeled results with different blooms cases.

2. Altimeter Waveform

2.1. Waveform Model

[7] The model of altimeter echo waveform from an extremely calm ocean surface and/or surface slick is based on the works of *Brown* [1977] and *Barrick and Lipa* [1985]. The altimeter radar cross section for backscatter is a function of time and can be expressed as [*Barrick*, 1972]

$$\sigma(t) = 2\pi^2 a^2 |R(0)|^2 \int_0^\infty g(\psi)(\sec\theta)^4 \sin\phi \cdot \left[\int_{-\infty}^{+\infty} P(\xi-\zeta) p_j(\xi) d\xi\right] d\phi, \quad (1)$$

where ζ is the sea surface elevation above the mean local surface, ψ is the angle at the antenna from nadir to a point ζ of the surface, ϕ is the angle at the earth center from the satellite to ζ, $g(\psi)$ is the two-way antenna normalized gain pattern, $P(x)$ is the normalized effective pulse shape as a function of spatial propagation distance, $x = (ct)/2$, a is the earth's radius, $R(0)$ is the Fresnel reflection coefficient of the sea surface at normal incidence, θ is the angle between the local normal to the surface at ζ and the satellite, and $p_j(\zeta)$ is the joint height-slope distribution probability density function at elevation ζ and wave slopes corresponding to specular angle θ.

[8] Assuming a Gaussian shape of standard deviation σ_τ for the antenna beam pattern g, a Gaussian shape of standard deviation u_b for the compressed altimeter pulse P and also a Gaussian joint probability of sea surface slope and elevation p_j, under the small angle approximation, the cross section σ simplifies to

$$\sigma\left(\frac{2x}{c}\right) = \frac{\pi^2 H'' |R(0)|^2 \sigma_\tau \sigma_0}{2\sigma_p} \int_0^\infty e^{-\frac{u}{u_b}} e^{-\frac{(x-u)^2}{2\sigma_p^2}} du, \quad (2)$$

where $u = (H'\psi^2)/2$, H' and H'' defined by $H' = H(1 + H/a)$ and $H'' = H/(1 + H/a)$ are the reduced and extended satellite heights, and u_b is defined by $u_b = (H'\psi_b^2)/2$, with $\psi_b = \psi_H/\sqrt{8\ln 2}$, ψ_H being the two-way half-power antenna beamwidth. Here σ_0 is the normal incidence surface cross section; σ_p is defined by $\sigma_p = \sqrt{h^2 + \sigma_\tau^2}$, and h is the RMS wave height. The different altimeter characteristics are given in Table 1.

[9] The simplest way to take into account σ_0 variations within the footprint is then to consider that σ_0 is compounded by a function $A(u, \theta)$. Equation (2) in then modified as

$$\sigma\left(\frac{2x}{c}\right) = \frac{\pi^2 H'' |R(0)|^2 \sigma_\tau \sigma_0}{2\sigma_p} \int_0^\infty e^{-\frac{u}{u_b}} e^{-\frac{(x-u)^2}{2\sigma_p^2}} \left[\frac{1}{2\pi}\int_0^{2\pi} A(u,\theta) d\theta\right] du. \quad (3)$$

For practical computation, A is expressed in the local altimeter coordinate (u, θ) using the following transform:

$$x = H\psi\cos\theta = H\sqrt{(2u)/H'}\cos\theta = \sqrt{2uH''}\cos\theta \quad (4)$$

$$y = H\psi\sin\theta = H\sqrt{(2u)/H'}\sin\theta = \sqrt{2uH''}\sin\theta. \quad (5)$$

Table 1. Operating Characteristics of Altimeters

Altimeter	TOPEX Ku	Jason Ku	Envisat Ku
Launch date	10 August 1992	7 December 2001	1 March 2002
Altitude, km	1334	1334	784
Inclination	66°	66°	98°
Beam width	1.1°	1.25°	1.33°
Frequency, GHz	13.60	13.575	13.575
PRF, Hz	4200	1800	1800
Bin width, ns	3.125	3.125	3.125
Waveform frequency, Hz	10	20	18
Number of waveforms in average	228	90	100

[10] The modulation can thus be expressed as

$$A(u,\theta) = A\left(\frac{x^2+y^2}{2H''}, \tan^{-1}\left(\frac{y}{x}\right)\right). \quad (6)$$

[11] Finally, the slope of the waveform plateau used in the altimeter waveform processing to estimate the off-nadir angle of the satellite, is also a good indicator of the waveform distortion. The square of the off-nadir angle, ν is defined by [*SSALTO Project*, 1999]

$$\nu^2 = \frac{1}{2(1+2/\gamma)}\left(1+\frac{-\beta}{\alpha\Delta t}\right), \quad (7)$$

where β is the slope of the plateau determined by linear regression of the plateau gates, $\gamma = (4/2 \log 2)(\sin(\phi_b/2))^2$ and $\alpha = 4(c/\gamma H')$. Negative values can occur and are kept in the GDR data set. In standard processing, the angle is estimated from the 1-s average waveform. The data editing for bad attitude only considers large positive off-nadir angles.

2.2. Estimation of σ_0 Variations

[12] It is well known that surface films dampen small-scale roughness at the ocean surface. Sea surface films represent the site of intense accumulation of organic matter from underlying waters. The damping mechanism depends upon the elasticity of the surfactants. The surface film elasticity modifies the molecular viscosity [*Levitch*, 1962] to enhance viscous dissipation of the short surface waves [*Kudryavtsev et al.*, 2005]. Especially under light wind conditions, small-scale roughness can be locally completely suppressed resulting in enhanced cross section at nadir (i.e., attenuation off nadir). At nadir, the microwave backscatter under light wind condition is inversely proportional to the mean squared variance of the surfaces slopes, but shall also depend strongly on the surface slopes densities. *Brown* [1979] suggests that a Laplacian density provides more consistent results than a Gaussian density for very low sea

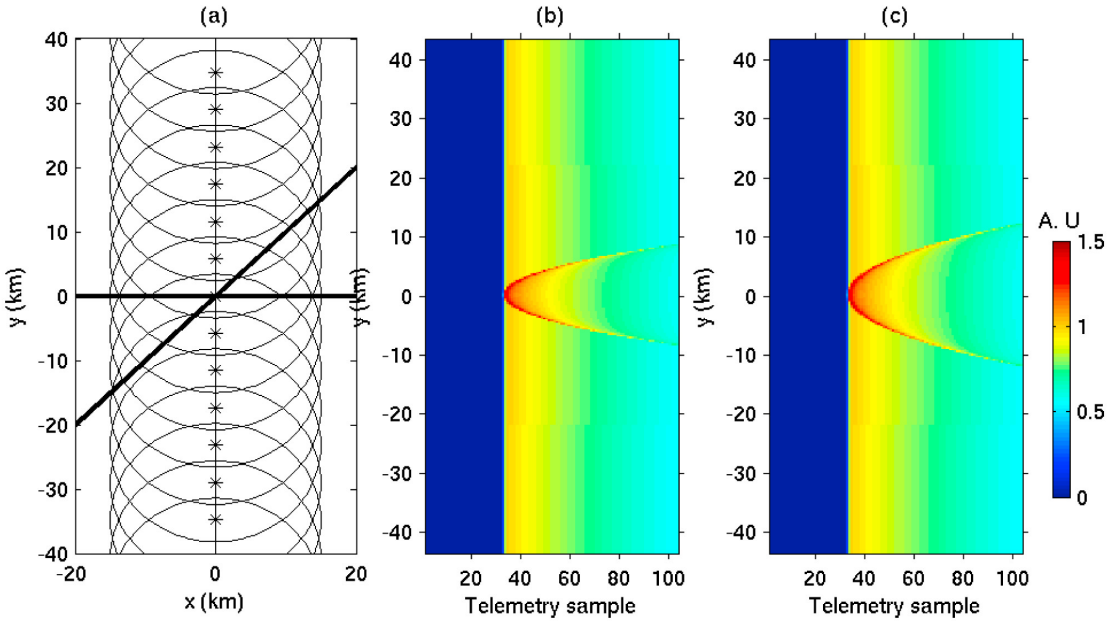

Figure 4. Jason altimeter echo waveforms in presence of simple surface slicks of 10 dB relative brightness and 100 m width. (a) Schematic diagram showing the slicks (thick solid lines) and the altimeter footprint (circles, 1 per second). Modeled waveforms for (b) perpendicular slick and (c) the 45° oblique slick. The waveform colorscale is in arbitrary units (1 corresponds to the maximum value of the Brown model).

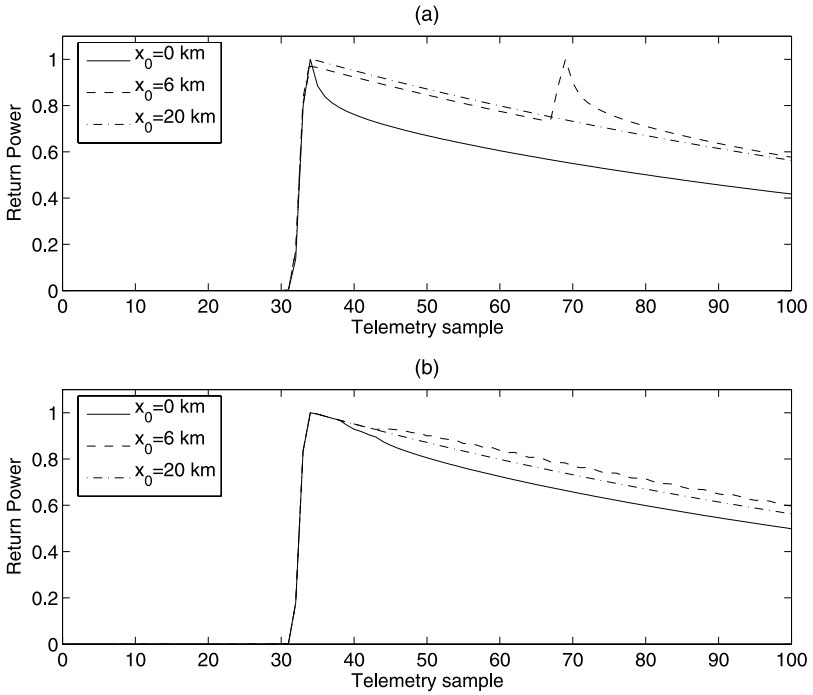

Figure 5. Jason altimeter normalized echo waveform in presence of a simple surface slick of 10 dB relative brightness and 100 m width. (a) High rate normalized waveforms for different distance x_0 between the satellite nadir and the slick. (b) The 1-s average normalized waveforms for the same x_0.

state condition. For a given slope variance, the resulting cross section is 3 times larger than for a Gaussian case. We further follow estimates from *Cox and Munk* [1954] analysis on glitter specular slope statistics stating that the slope variance can easily be divided by 3 between clean and slick surface. Consequently, the expected relative contrast at nadir between clean and slick area may easily reach 10 dB within the altimeter footprint. Such an enhanced contrast

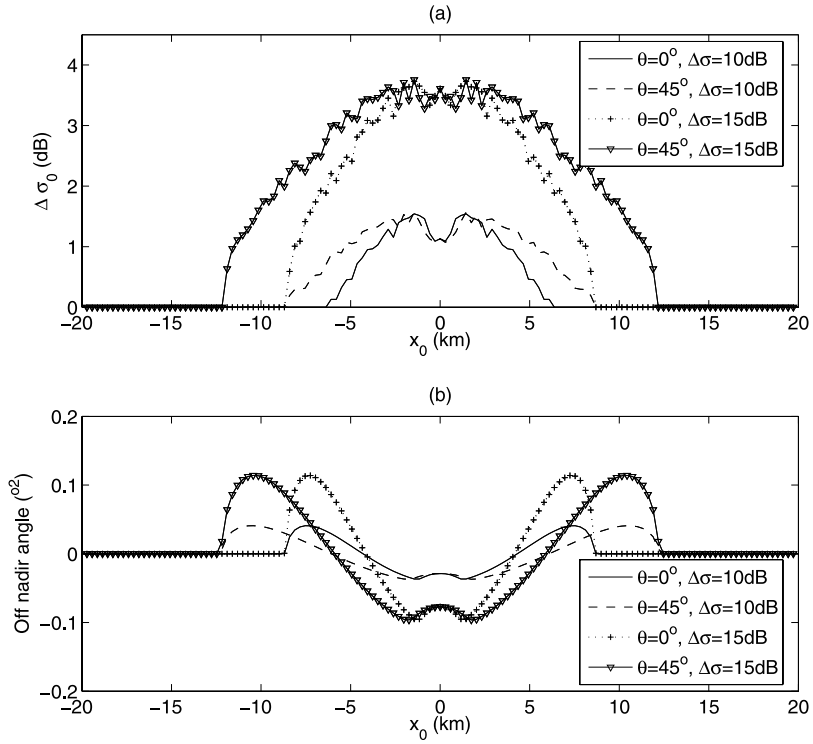

Figure 6. (a) Variation of σ_0 induced by the linear slick for different angles and relative brightness. (b) Variation of off-nadir angle estimates.

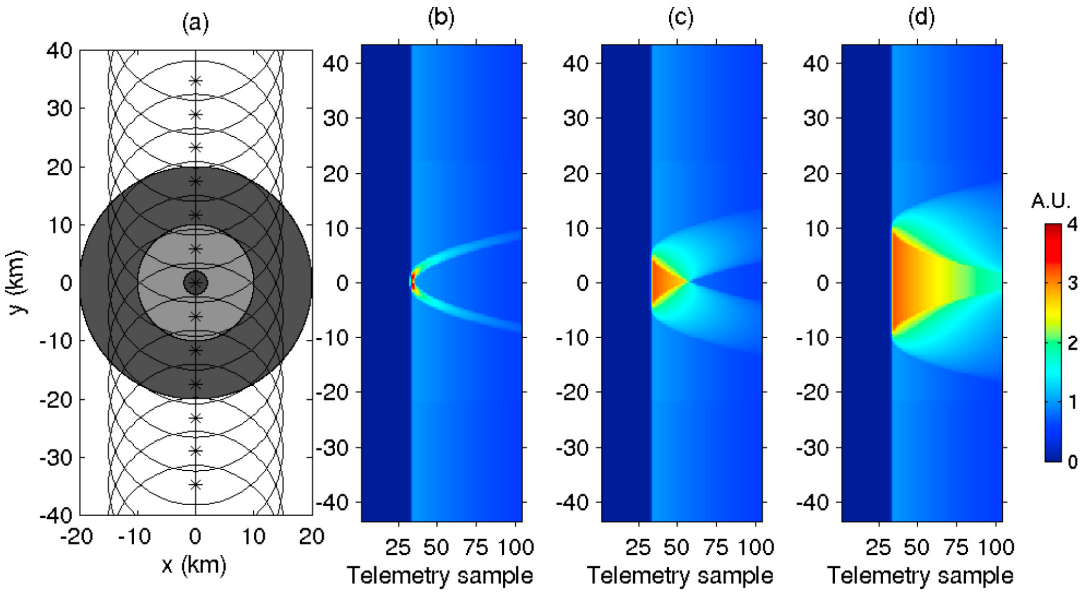

Figure 7. Jason altimeter echo waveform in presence of circular slicks of 2 and 10 km radius and 10 and 5 dB relative brightness. (a) Schematic diagram showing the slicks (gray circles) and the altimeter footprint (circles, 1 per second). Modeled waveforms for the (b) 2 km radius and 10 dB brightness slick, (c) 10 km radius and 5 dB brightness slick, and (d) 20 km radius and 5 dB brightness slick. The waveform colorscale is in arbitrary units (1 correspond to the maximum value of the Brown model).

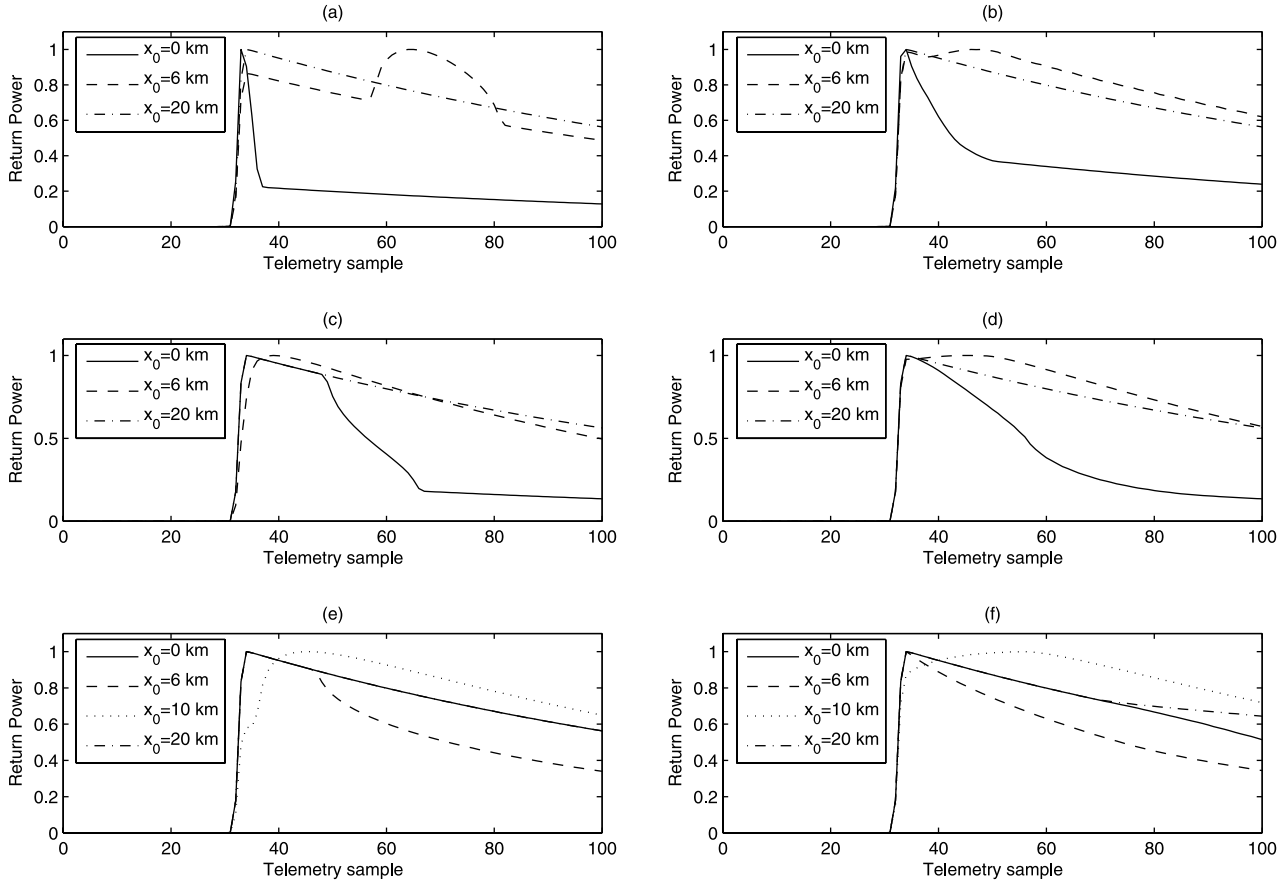

Figure 8. Jason altimeter normalized echo waveform in presence of circular surface slicks. (a) High rate waveforms for different distances x_0 between the satellite nadir and the slick, and (b) 1-s average waveforms for the same x_0 for the 2 km radius 10 dB slick. Same as Figures 8a and 8b, respectively, for (c, d) a 10 km radius 5 dB slick and (e, f) a 20 km radius 5 dB slick.

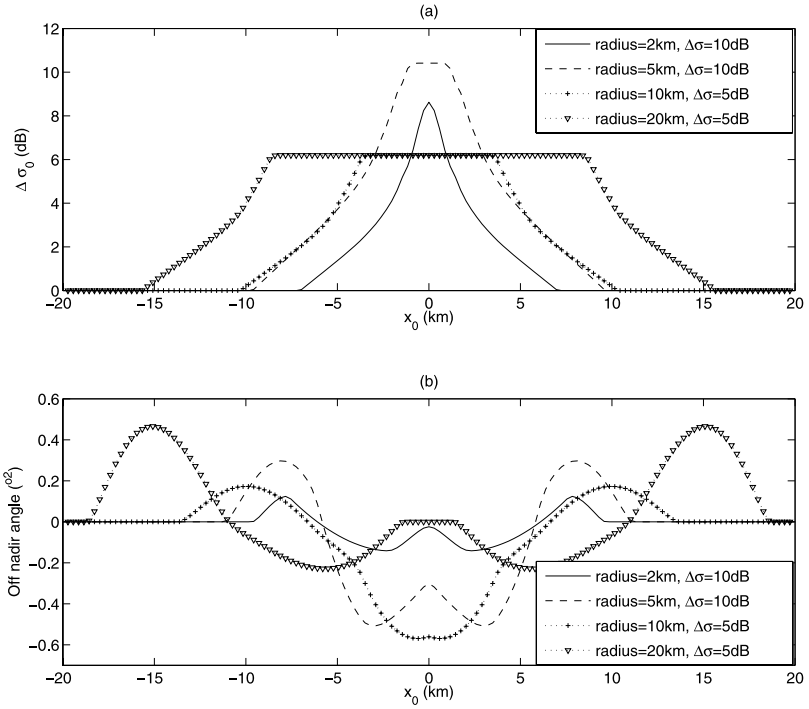

Figure 9. (a) Variation of σ_0 induced by the slick for different radii and relative brightness. (b) Variation of off-nadir angle estimates.

will be used to model the impact of a bloom event on the altimeter waveforms.

3. Modeling Bloom Event

3.1. Simple Surface Slick

[13] In a first-order approximation, a surface slick is considered as a reflective (bright) straight line of width l and infinite length (see Figure 2). The modulation function A for such a feature becomes

$$A(u,\theta) = A_0\left[\arccos\left(\frac{H'(x_0-l)}{2Hu}\right) - \arccos\left(\frac{H'(x_0+l)}{2Hu}\right)\right], \quad (8)$$

where A_0 is the slick contrast (relative to the background) and x_0 is the distance between satellite nadir and slick.

[14] Figure 4 presents the modeled waveforms for a surface slick of 100 m width, infinite length, and 10 dB relative contrast. Two cases are considered, slicks perpendicular to the satellite track and oblique at 45° angle. As expected, the waveform fields present the V-shaped patterns over the slicks. As the altimeter footprint approaches and passes over the slick, the increase of return power resulting from the enhanced backscatter areas moves from the tail of the waveform toward the peak and then away from it. The width of the parabola described by the return power maximum increases when the slick becomes parallel to the satellite track. For a slick perpendicular to the satellite ground track, the effect of the slick is only significant over a short distance (of about 20 km, i.e., about 4 s of data).

[15] Depending on the distance x_0 between the satellite nadir point and the slick, the waveform is more or less distorted as can be seen in Figure 5. For small x_0, the waveform peak strongly increases and the plateau decay becomes very rapid. For higher x_0, only the outer edge of the altimeter footprint is concerned. The impact of the slicks becomes smaller and only affects the trailing edge of the waveforms. If 1-s average waveforms are considered, the effect is only noticeable for the sample where the slick is located at the satellite nadir ($x_0 = 0$). The mean effect is a slight increase of the peak and a slightly more rapid decay of the plateau.

[16] The modification of measured backscatter by such a small slick is about 1.5 dB and can reach 4 dB for a relative brightness of 15 dB (see Figure 6). As the waveform shape is strongly modified, the off-nadir angle estimates yield strong variations with a positive-negative-positive oscillation. The amplitude of the oscillation depends on the relative slick brightness and can reach $\pm 0.12^{\circ 2}$.

3.2. Circular Patches

[17] Patches of reduced backscatter in SAR imagery under low wind speed conditions can be represented by reflecting disks of constant relative brightness. The σ_0 modulation for such a pattern can be expressed as

$$A(u,\theta) = A_0 \arccos\left(\frac{uH^2/H' + x_0^2 - d^2}{2x_0H\sqrt{(2u)/H'}}\right), \quad (9)$$

where x_0 is the distance between the satellite nadir and the patch center and d is the patch diameter.

[18] The signature of small patches is similar to the linear slick ones with a V-shaped enhancement (see Figure 7). The enhancement is higher and more concentrated where the slick is directly located at the satellite nadir (see Figure 8).

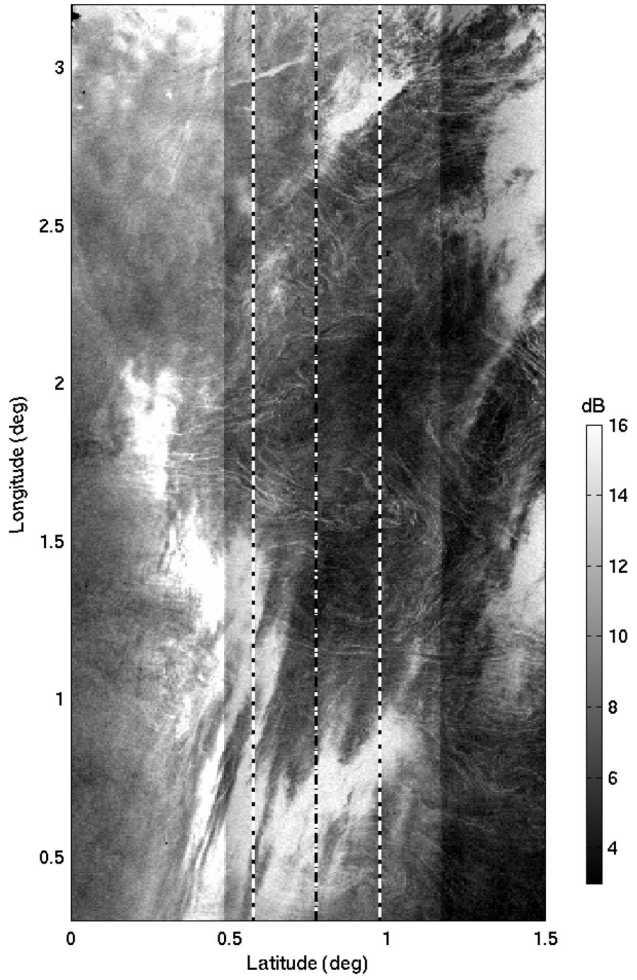

Figure 10. Surface σ_0 in dB estimated from the Envisat SAR image of Figure 2. The dash-dotted line represents the altimeter ground track, and the dotted line represents the altimeter footprint.

For larger patches, the V-shaped pattern is still present but more diffuse and a triangular pattern appears near the satellite nadir. This kind of pattern can also be observed in the Jason waveform in Figure 1 near 1.4°S. When the patch diameter becomes of the same order of magnitude as the altimeter footprint (about 20 km), the waveform is only strongly distorted on the outer edges of the patch. When the patch is located at nadir the waveform regains the standard Brown model shape.

[19] The 1-s averaged waveforms also presented in Figure 8 show that there is a striking likeness between the 1-s average for a 20-km patch and the mean waveforms sorted by off-nadir angle presented in Figure 3b. The distortion of the waveform strongly depends on the relative surface NRCS variation within the altimeter footprint. It can thus be expected that the altimeter tracker will lose lock directly over small slicks or patches and on the edge of larger patches. This appears to be the case for Jason tracker near 1°S for a large patch and near 1.7°S for a small one.

[20] When the surface area of the patch is of the same order of magnitude as the altimeter footprint, the increase of backscatter is equal to the relative patch brightness as can be seen in Figure 9. The estimate of the off-nadir angle presents the same positive-negative-positive oscillation as in the simple case but the variation amplitude is larger and can reach $0.5^{\circ 2}$ for large patches. Such a large oscillation can also be seen in Figure 2 for Jason waveforms near 1.7 and 1.4°S.

3.3. σ_0 From SAR Images

[21] A final model was generated for realistic surface NRCS variation estimated from SAR image under low wind condition. Figure 10 presents the surface σ_0 used to model the waveforms along with a Jason type altimeter track represented by the dashed line. This fields contains large strongly reflective patches near 0.7 and 2.7° as well as a number of slick-like features between 1 and 2.5°. The σ_0 contrasts used to model the waveforms have been directly deduced from the measured contrast in SAR image intensities. This development follows the expected slope variance reduction following the *Kudryavtsev et al.* [2005] radar imaging model based on *Ermakov et al.* [1992] surface slick elasticity model. Under light winds ($\leq$5 m/s), short gravity waves can be totally suppressed, resulting in σ_0 drops in SAR images and thus σ_0 increases at nadir. The modeled waveforms are presented in Figure 11. The likeness of the modeled waveforms patterns with those of Figure 2 is striking. The large triangular patterns of high return power such as the one near 0.75° associated with the large patches strongly resemble those of Figure 2 near 2°S and 1°S. The small slicks result in V-shape patterns more or less bright depending on their width and relative brightness. Their signatures sometimes blend, like near 1.5°, smoothing the V-shape patterns. Such merging can also be observed in Figure 2 between 0.9 and 0.6°S.

[22] The increase of backscatter also presented in Figure 11 presents large variations similar to the measured ones of Figure 2 and oscillated between 0 and 10 dB. The large patch located near 0.5° gives an increase of about 10 dB over more than 75 km, an order of magnitude in amplitude and length similar to the one observed near 1°S in Figure 2. The off-nadir angle takes large positive values at the edges of the patches and slicks and stays small or negative within the patches. The relative maxima of σ_0 increase are thus associated with small or negative off-nadir angle value. The behavior of the mean modeled waveforms sorted by σ_0 or off-nadir angle is similar to the measured mean ones (see Figure 12).

4. Analysis of Waveforms During σ_0 Bloom Events

[23] As a final validation of the model, bloom events have been analyzed in terms of changing surface σ_0. A minimization procedure similar to the one used to estimate rain cell characteristics from altimeter waveforms [*Tournadre*, 1998] is used to determine the model's best fit to the observed waveforms. The method minimizes the distance between modeled and measured waveforms. Figure 13 presents the results of the minimization procedure for the feature observed near 1.4°S in Figure 2. The best fit corresponds to an 8 km, 4.7 dB relative brightness circular patch. The waveform pattern is well reproduced considering the high noise level of the measured waveforms. This patch corresponds to

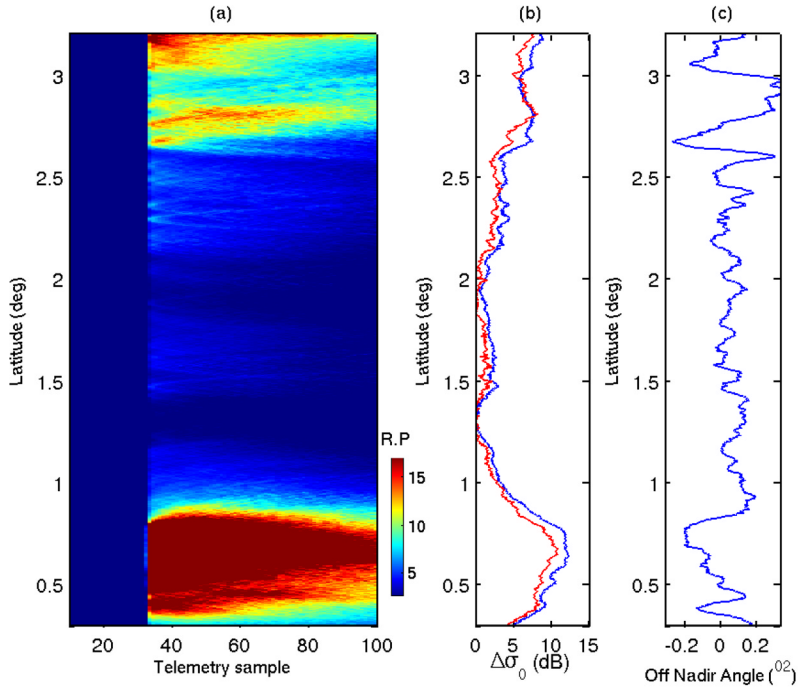

Figure 11. (a) Modeled waveforms for a Jason type altimeter using the surface σ_0 of Figure 10; the colorscale is in Arbitrary units. (b) Relative variation of σ_0 estimated from the waveforms (blue line) and mean surface σ_0 over the altimeter footprint. (c) Estimate of off-nadir angle.

σ_0 increase of 4.7 dB and to a variation of the off-nadir angle between -0.5 to $0.4^{\circ 2}$.

[24] Figure 14 presents the best fit of a small bloom event detected in the Jason pass 47 of cycle 107 off the coast of Sumatra near 2.2°N. The measured σ_0 was above 20 dB over about 10–20 km. The measured waveforms shown in the figure present a sharp V-shaped pattern which corresponds to a relative σ_0 change of 2dB and an off-nadir variation of $\pm 0.2^{\circ 2}$. A linear slick of 100 m width and 15 dB relative brightness gives the best fit of the model. The figure shows good agreement between the measured and modeled waveforms. It also shows that the model reproduces well the σ_0 and off-nadir angle variations.

[25] The last example, which corresponds to a more complex situation where the signature from different surface patterns merge, is taken from the Envisat RA2 archive. A

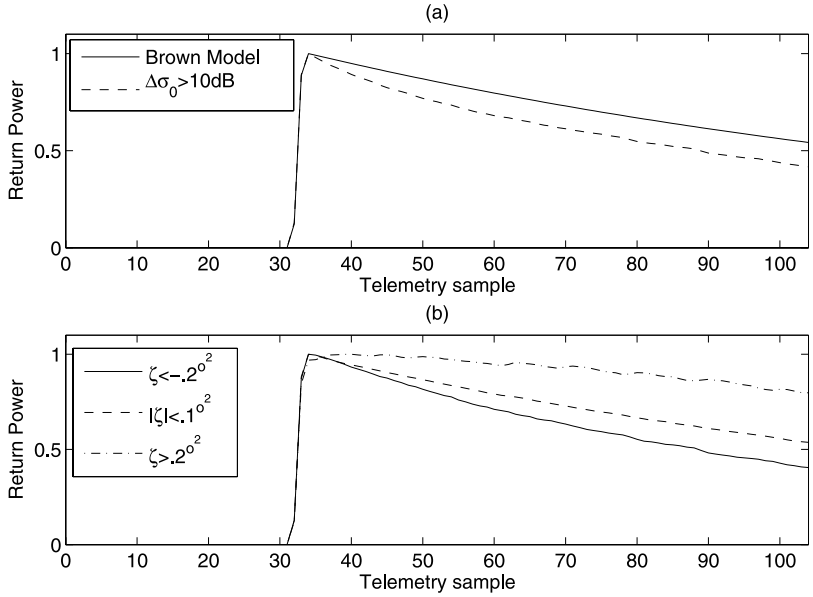

Figure 12. Mean normalized altimeter waveforms of Figure 11, (a) sorted according to σ_0 and (b) sorted according to off-nadir angle.

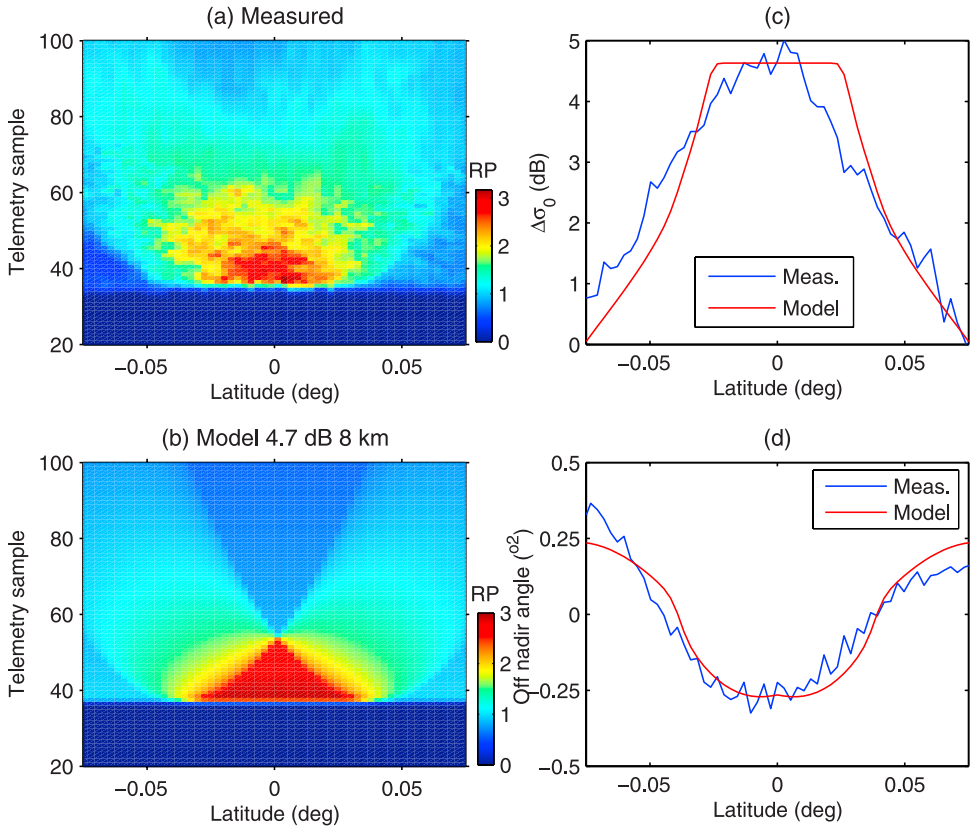

Figure 13. Best fit of observed waveforms. (a) Jason waveforms near 1.4°S for cycle 107 pass 14, (b) modeled waveforms for a 8 km, 4.7 dB relative brightness circular patch, (c) observed and modeled relative σ_0 variation, and (d) observed and modeled off nadir angle. The waveform colorscale (R.P., i.e., Return Power) is in arbitrary units.

bloom was detected south of the Andaman and Nicobar Islands in the Indian Ocean on pass 94 cycle 10 (2002/10/04) near 7°N where σ_0 largely exceeds 15 dB over about 100 km. The waveforms presented in Figure 15 show the complex patterns of merging V-shaped patterns at the edge of the bloom near 6.7°N. Two marked ones can be easily discerned. A best fit was performed separately on these two features with the following results, a 2 dB 2 km circular patch for the southernmost, and 9 dB and 1 km for the northernmost.

5. Conclusion

[26] Sea level data from all satellite altimeters currently in operation (Jason, TOPEX/Poseidon, Envisat RA2) are often degraded concurrently with events of very high radar cross section. These events, termed σ_0 blooms in the literature which affect about 5–6% of the over-ocean TOPEX data, are likely associated with no or low wind speeds [*Mitchum et al.*, 2004]. A detailed analysis of the TOPEX archive [*Mitchum et al.*, 2004] reveals that about 60% of the affected data are rejected by the recommended TOPEX data flagging.

[27] We present an analysis of σ_0 blooms using the high-resolution waveforms given in the Sensor Data Records of the altimeters. Examples of waveforms presented in Figure 1 show the wealth of information they contain. The distortion of the waveforms, which leads to tracker loss, is often associated with V-shaped patterns. These are characteristics of surface variations at scales smaller than the altimeter footprint. On the basis of the experience already gained through the analysis of high-resolution altimeter waveforms in presence of rain cell, a model is developed.

[28] This model is applied to simple patterns, namely linear infinite slick and circular patches. The results confirm the strong distortion of the waveforms by highly reflecting localized patches and slicks. The distortion is, in general, more important at the edges of the slick/patches as shown by the large fluctuations of the off-nadir angle in these zones. In such cases, it is almost impossible to retrieve meaningful geophysical parameters even when retracking the waveforms. However, when the highly reflecting area becomes of the same order or larger than the altimeter footprint, a Brown model is still valid and the waveforms present little distortion within the patch. This explains why about 40% of the measured waveforms during blooms are not flagged. They are in fact still valid for geophysical parameters estimates and should therefore not be flagged. A flag based on a σ_0 threshold only is thus certainly not adapted to eliminate erroneous data during bloom events. A reliable one can be defined using threshold values (especially negative) of the off-nadir angle estimate. Another interesting feature of these waveforms that are not affected by distortion is that, following the *Brown* [1979] suggestion, they can be used to assess the slope density estimates for low wind sea conditions.

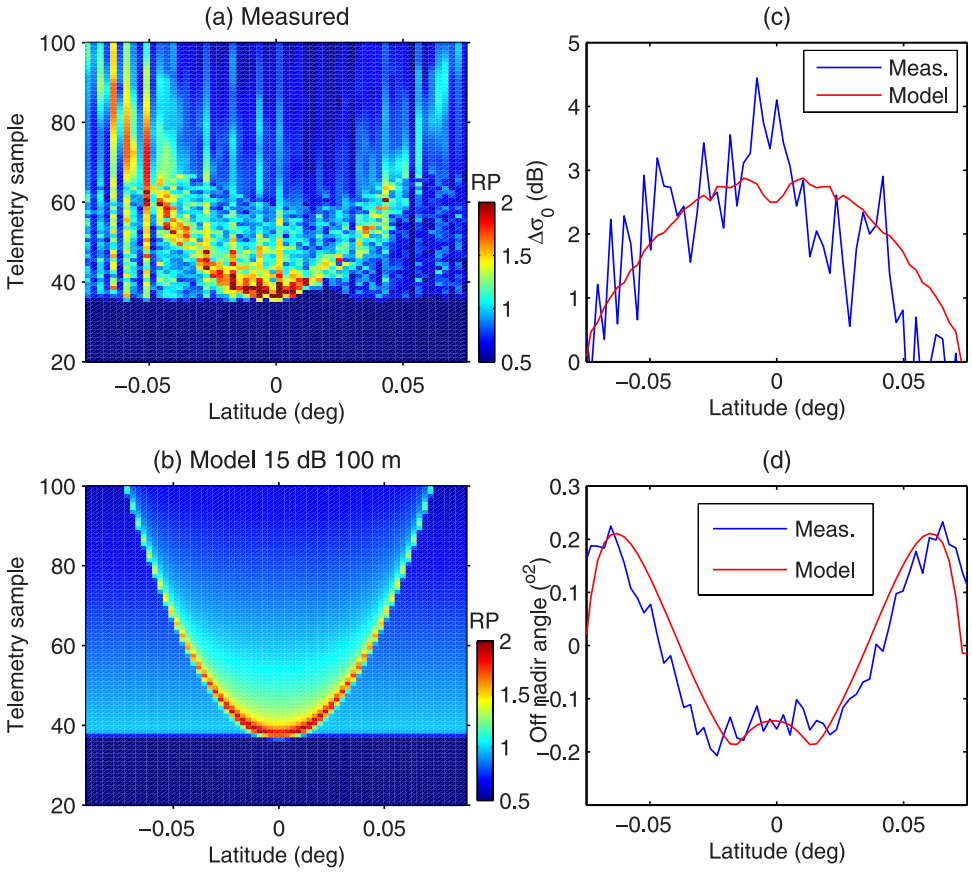

Figure 14. Best fit of observed waveforms. (a) Jason waveforms near 1.4°S cycle 107 pass 34, (b) modeled waveforms for a 100 m, 15 dB relative brightness linear slick, (c) observed and modeled relative σ_0 variation, and (d) observed and modeled off-nadir angle. The waveform colorscale is in arbitrary units.

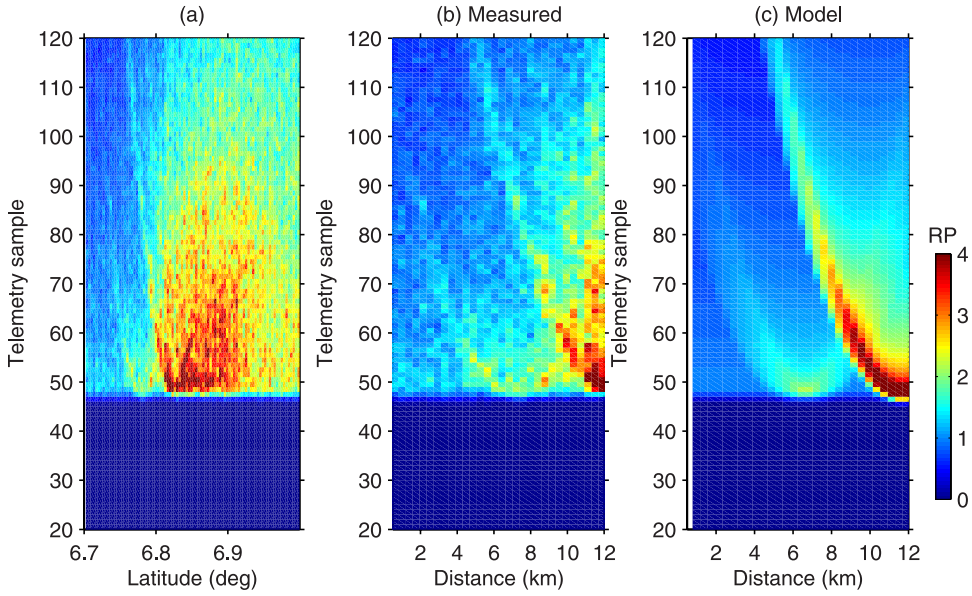

Figure 15. Best fit of observed waveforms. (a) Envisat waveforms near 6°N–7°N for cycle 10 pass 94. (b) Details of the waveforms near 6.7°N showing the two V-shaped patterns. (c) Modeled waveforms. The waveform colorscale is in arbitrary units.

[29] Using SAR imagery under low winds conditions, which presents both linear slicks and large patches, nadir σ_0 has been estimated and used as input to the waveform model. The resulting waveforms are qualitatively very similar to the measured ones. Their mean behavior, sorted either by relative σ_0 or off-nadir angle, is identical to the measured ones.

[30] Accordingly, the small-scale variations of surface σ_0 can explain the behavior of altimeter waveforms in bloom events. On the basis of these results, use of the high-resolution altimeter waveforms may offer an interesting mean to study marine slick occurrence rates as well as type, using the expected σ_0 contrast. As for oceanic rain, it is foreseen that one can build a slick climatology within different chosen regions. These climatologies could then be profitably compared with the regions of reduced backscatter observed in scatterometer data which have been associated with natural surface slicks by comparison with ocean color data [*Lin et al.*, 2003; *Hashizume and Liu*, 2004].

[31] **Acknowledgments.** This study was supported by CNES, ESA, and NASA. The Sensor Data Records necessary for the study were provided by the AVISO Centre.

References

Barrick, D. (1972), Remote sensing of sea state by radar, in *Remote sensing of the troposphere*, chap. 12, pp. 12-1–12-46, U.S. Gov. Printing Off., Washington, D. C.

Barrick, D., and B. Lipa (1985), Analysis and interpretation of altimeter sea echo, *Adv. Geophys.*, *27*, 61–100.

Brown, G. S. (1977), The average impulse response of a rough surface and its applications, *IEEE Trans. Antennas Propag.*, *AP-25*, 67–74.

Brown, G. (1979), Estimation of surface wind speed using satellite-borne radar measurements at normal incidence, *J. Geophys. Res.*, *84*, 3974–3978.

Clemente-Colón, P., and X.-H. Yan (2000), Low backscatter features in SAR imagery, *Johns Hopkins APL Tech. Dig.*, *21*(1), 116–121.

Cox, C., and W. Munk (1954), Statistics of the sea surface derived from Sun glitter, *J. Mar. Res.*, *13*, 198–227.

Ermakov, S., S. Salashin, and A. Panchenko (1992), Film slicks on the sea surface and some mechanisms of their formation, *Dyn. Atmos. Ocean*, *16*, 279–304.

Hashizume, H., and W. T. Liu (2004), Systematic error of microwave scatterometer wind related to the basinscale plankton bloom, *Geophys. Res. Lett.*, *31*, L06307, doi:10.1029/2003GL018941.

Kudryavtsev, V., D. Akimov, J. Johannessen, and B. Chapron (2005), On radar imaging of current features: 1: Model and comparison with observations, *J. Geophys. Res.*, *110*, C07016, doi:10.1029/2004JC002505.

Levitch, V. (1962), *Physicochemical Hydrodynamics*, Prentice-Hall, Upper Saddle River, N. J.

Lin, I., W. Alpers, and W. T. Liu (2003), First evidence for the detection of natural surface films by the QuikSCAT scatterometer, *Geophys. Res. Lett.*, *30*(13), 1713, doi:10.1029/2003GL017415.

Mitchum, G., D. Hancock, G. Hayne, and D. Vandemark (2004), Blooms of sigma0 in the TOPEX radar altimeter data, *J. Atmos. Oceanic Technol.*, *21*, 1232–1245.

SSALTO Project (1999), *Algorithm Definition, Accuracy and Specification*, vol. 2 *CMA Altimeter Level 1B Processing*, *Tech. Rep. SMM-ST-M2-EA-11003-CN*, Cent. Natl. d'Etudes Spatiales, Toulouse, France.

Tournadre, J. (1998), Determination of rain cell characteristics from the analysis of TOPEX, *J. Atmos. Oceanic Technol.*, *15*, 387–406.

Tran, N., D. W. I. Hancock, G. S. Hayne, D. W. Lockwood, D. Vandemark, M. L. Driscoll, and R. V. Sailor (2002), Assessment of the cycle-to-cycle noise level of the Geosat Follow-On, TOPEX, and Poseidon altimeters, *J. Atmos. Oceanic Technol.*, *19*, 2095–2107.

B. Chapron, N. Reul, and J. Tournadre, Laboratoire d'Océanographie Spatiale, Institut Français de Recherche pour l'Exploitation de la Mer, Technopôle de la Pointe du Diable, 29280, Plouzané, France. (jean.tournadre@ifremer.fr)

D. C. Vandemark, NASA Goddard Space Flight Center, Wallops Island, VA 23337, USA.